JOURNAL OF PROPULSION AND POWER
Vol. 28, No. 3, May–June 2012

Scaling of Efficiency with Applied Magnetic Field in Magnetoplasmadynamic Thrusters

Dan R. Lev* and Edgar Y. Choueiri†
Princeton University, Princeton, New Jersey 08544

DOI: 10.2514/1.B34194

An investigation of the scaling of thrust efficiency with the applied magnetic field in applied-field magnetoplasmadynamic thrusters is carried out in order to provide guidelines for scaling and controlling applied-field magnetoplasmadynamic thruster performance. Thruster voltage measurements were made at different current, applied-magnetic-field, and mass-flow-rate levels in a 30 kW lithium-fed applied-field magnetoplasmadynamic thruster. The efficiency was then calculated using the voltage data along with a semiempirical thrust formula derived and verified previously for the same thruster. The nonuseful voltage component (the voltage associated with the thruster's power losses) was found to scale linearly with the current and applied magnetic field and inversely with the mass flow rate. This behavior was attributed to electrode sheath effects and decreased conductivity with an increasing applied magnetic field. The efficiency was found to increase with the applied magnetic field for all current and mass-flow-rate values, and the enhancement of the efficiency by the applied magnetic field was found to be greater when the mass flow rate was reduced. The observed minimum in the efficiency versus the current curve was related to the interplay between the components of the thrust and was shown experimentally and analytically to increase with increasing the applied field and decreasing the mass flow rate.

Nomenclature

B	=	magnetic field, T
g_0	=	standard gravity constant, 9.81 m/s^2
J	=	current, A
$\dot{m}$	=	mass flow rate, mg/s
P	=	electrical power, W
r	=	radius, mm
T	=	thrust, N
u_e	=	exhaust velocity, m/s
V	=	voltage, V
η	=	efficiency

Subscripts

a	=	anode
c	=	cathode
E	=	electrodes
emf	=	electromotive force
gd	=	gas dynamic
H	=	Hall
res	=	resistive
self	=	self-induced magnetic field

I. Introduction

MAGNETOPLASMADYNAMIC thrusters (MPDTs) are a subclass of plasma thrusters with an overwhelmingly electromagnetic acceleration mechanism involving the interaction of a current between an anode and a cathode and a magnetic field, which could be applied or induced by the current itself. This interaction gives rise to a Lorentz force density ($f = j \times B$) that accelerates propellant downstream and out of the thruster. High thrust and thrust density are also the big advantages that MPDTs have over other types of electric propulsion devices, such as the Hall thruster or the ion thruster. MPDTs promise a wide range of thrust levels (100 mN–100 N) [1–3], depending on the power level, along with high specific impulse (1000–5000 s), a high thrust efficiency (10–25% with argon and up to 60% with lithium propellant), and the ability to process hundreds of kilowatts in a single compact device.

The thrust-generation mechanism of the self-field MPDT is well understood; it was characterized by Maecker [4] and Jahn [5] and analyzed by Choueiri [6], who showed how the various components of thrust scale with geometric and operational parameters. It has been well established [1] that the addition of an applied magnetic field to the thruster increases its performance significantly. This is often necessary at low power levels (usually below 100 kW) where the current is too low for the self-induced magnetic field to be sufficient. Thrust, efficiency, and specific impulse tend to increase with the applied-magnetic-field intensity. It has been observed [1] that the thrust increases linearly with the product JB, where J is the total current applied to the thruster, and B is the value of the applied magnetic field measured at the solenoid's center. This linear increase region with JB depends on the mass flow rate, thruster geometry, and propellant used. This linear increase is not similar to the thrust increase in self-field MPDTs where the thrust scales with the current squared (J^2), thus implying a different acceleration mechanism between the two types of thrusters. For example, unlike in self-field MPDTs, the addition of an applied magnetic field creates an azimuthal force density component that swirls the plasma and is responsible for affecting kink instabilities differently than observed in self-field MPDTs [7]. For the aforementioned reasons, applied-field MPDTs (AF-MPDTs) can operate at power levels much lower than self-field MPDTs. In addition, thrust efficiencies in AF-MPDTs were reported to be significantly larger [2,3]. The detailed physics behind the acceleration mechanism in AF-MPDTs is not yet fully understood, and further experimental research is needed.

The focus of ongoing studies on AF-MPDTs is on the most promising variant called the lithium Lorentz force accelerator (LiLFA). The LiLFA is a steady-state AF-MPDT that uses lithium as a propellant and a MCHC, through which the lithium vapor propellant is injected into the thruster's acceleration region. Lithium has great potential for two main reasons:

1) Lithium's first ionization potential (5.4 eV) is significantly lower than that of other, commonly used propellants such as argon (15.7 eV), xenon (12.1 eV), or hydrogen (13.6 eV), while lithium's

Presented as Paper 2010-7024 at the 48th Joint Propulsion Conference, Nashville, TN, 25–28 July 2010; received 29 November 2010; revision received 30 June 2011; accepted for publication 22 August 2011.

*Graduate Research Assistant. Student Member AIAA.
†Chief Scientist, Electric Propulsion and Plasma Dynamics Laboratory, and Professor, Applied Physics Group, Mechanical and Aerospace Engineering Department. Fellow AIAA.

second ionization potential is significantly higher than that of these propellants. Therefore, the frozen flow losses are expected to be lower in lithium-fed MPDTs.

2) Lithium (especially with the addition of small amounts of barium) lowers the work function of the thruster's cathode, thus enabling cathode operation at much lower temperatures [8] and reducing cathode erosion. The above two advantages make lithium a very good candidate for high-power AF-MPDTs. Lithium-fed MPDTs have high efficiencies, in the range of 20 to 60% depending on the power level, and due to their low electrode erosion rate (when trace amounts of barium are added to the propellant), have demonstrated hundreds of hours of high-power operation (0.5 MW) without showing significant damage, such as electrodes' erosion, cathode wear, and diffusion welding of the cathode end [9,10].

The voltage-current V-J characteristics of the MPDT are important in evaluating the scaling of thrust efficiency in different operating regimes. The thrust efficiency is defined as the ratio between thrust power and total power. The total power is simply the product JV, thus emphasizing the importance of the V-J characteristics. Changing the applied current, mass flow rate, or applied magnetic field affects such plasma properties as the plasma resistivity and exhaust velocity. This in turn changes the required voltage to sustain operation and the generated thrust, leading to variations in efficiency for different operational regimes.

Previously, voltage models were sought in order to determine how the thruster's efficiency changes with operation and thruster parameters. Tikhonov et al. [2] suggested a semiempirical voltage model that is difficult to implement, as it requires experimental measurements of the electrodes' sheaths and knowledge of the electron temperature. Mikellides and Turchi [11] suggested and verified another analytical model, but the experimental data with which it agrees span a narrow spectrum of voltage-current behavior.

In this study, we perform a qualitative and experimental investigation of the voltage-current and efficiency-current characteristics in the LiLFA with the aim of shedding more light on the variation of efficiency with operating parameters in varying regimes. First, we measure the voltage of the LiLFA over a wide range of current, applied-magnetic-field, and mass-flow-rate values. Then, in order to calculate the thrust efficiency, we use a semiempirical expression for thrust derived by Popov et al. [10] that is based on, and verified by, previous experimental studies performed on the LiLFA. With the resulting extensive database in hand, we analyze the observed trends of the efficiency with the current, the applied magnetic field, and the mass flow rate and offer detailed physical interpretations to explain the observations.

II. Experimental Setup

A. Steady-State Low-Power Facility

All experiments were performed in the steady-state low-power (SSLP) facility at the Electric Propulsion and Plasma Dynamics Laboratory (EPPDyL) at Princeton University. The SSLP facility consists of a large cylindrical vacuum chamber, 1.5 m in diameter and 3.6 m long, made of stainless steel in order to withstand high temperatures. An active cooling jacket uses chilled water to maintain a moderate temperature along the chamber's inner walls. The ultimate vacuum of this system is 1.7×10^{-5} torr (2.266×10^{-3} Pa) and is obtained using a 1.22 m CVC-type PMC-48C (95, 000 l/s) diffusion pump, a Leybold Vacuum Products, Inc., RUVAC WSU-2000 1342 ft^3/min . (630 l/s) roots accelerator, and a 150 CFM (71 l/s) Stokes Microvac mechanical pump. All three pumps are connected to the vacuum chamber in series. Low pressure is easily kept during thruster operation, since lithium is solid at room temperature and therefore condenses on the inner walls of the vacuum chamber. Therefore, pressure could be kept at the ultimate pressure during firing.

An ingot of about 150 g of lithium is loaded into a small stainless steel reservoir, 80 mm in diameter and 166 mm in length. We perform the loading of the reservoir under an argon atmosphere in a glove box in order to keep the lithium in an inert environment. The reservoir is then attached to the thruster feeding system (Fig. 1) in the vacuum chamber, which is then closed and pumped down while a steady flow of argon in the reservoir keeps the lithium from reacting with air.

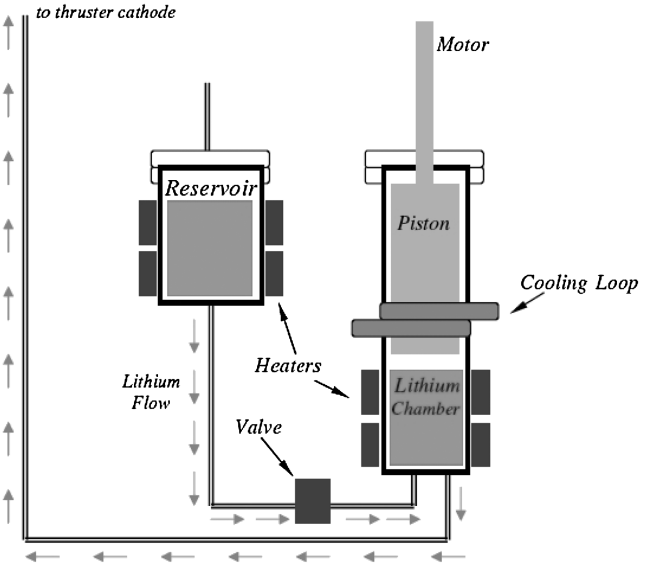

Fig. 1 LiLFA lithium feed system. Lithium flows from the reservoir to the cylinder where it is pushed by the piston through the pipeline and into the thruster cathode.

B. Lithium Propellant Supply

The lithium is fed through a dedicated feed system that is located in the vacuum chamber and for which the design and calibration were discussed by Kodys et al. [12]. Once brought to its melting temperature, lithium flows out of the reservoir and into a cylinder where it awaits ejection by a piston for which the position is carefully controlled. Once forced out of the cylinder, liquid lithium flows through a stainless steel $\frac{1}{4}$ in. pipe to the thruster's cathode where it is vaporized by a heater inside the cathode. The entire feed system requires about 1 kW of electric power and is controlled by four variacs to maintain a temperature of about 250°C during steady-state operation, about 70°C above lithium's melting temperature.

The lithium mass flow rate is directly proportional to the piston's velocity inside the cylinder [12] and can be varied within a range of 1–200 mg/s. Operation of the thruster itself is accomplished using a Miller SRS-1000 30 kW generator capable of supplying dc current up to 1500 A.

C. Thruster

The LiLFA (Fig. 2) was built and initially tested at Moscow Aviation Institute (MAI). It was transferred to Princeton University's EPPDyL in 1998. It consists of a conical anode made of tungsten with an upstream inner diameter of 45 mm and a downstream inner

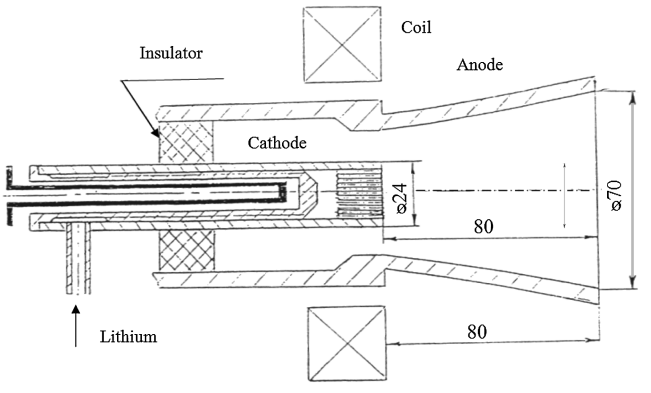

Fig. 2 Cross-sectional view of the LiLFA (all dimensions are in millimeters).

diameter of 70 mm. The cylindrical multichannel hollow cathode (MCHC), also made of tungsten, has an inner diameter of 19.2 mm and a length of 215 mm (100 mm in the thruster cavity). Its tip consists of 68 small rods, each 2 mm in diameter and 14 mm in length. Before thruster initiation, the cathode evaporates the incoming liquid lithium provided by the feed system due to a high initial temperature of well over 1000°C maintained by a graphite heater that is embedded inside the cathode and requires approximately 1.2 kW of power.

During operation, the cathode reaches temperatures of well over 2000°C [13], while the anode reaches temperatures of up to 2000°C [14].

The applied magnetic field is generated by a water-cooled solenoid, 280 mm in outer diameter and 120 mm in inner diameter. The solenoid consists of a copper tube 8 mm in diameter, which is turned 56 times in order to generate magnetic field values up to 0.08 T with a current of 250 A. At this operational point, the solenoid requires approximately 2.6 kW of power.

Since no effort was made to optimize the power consumption of the solenoid and lithium feed system, and since that consumption would depend on design considerations that are largely extraneous to the plasma dynamics of the discharge inside the thruster, the required power to operate these supporting subsystems was not included in the calculation of the thrust efficiency reported in this paper. However, we emphasize that, in this type of system, these additional power consumption requirements will have an effect on the overall system efficiency and must be taken into account in any final engineering design. In the LiLFA system, the solenoid and lithium preheating subsystems require about 2 kW each.

D. Voltage and Current Measurements

Total thruster voltage was measured across the anode and cathode through a voltage divider that matches the impedance of the data acquisition system. The total thruster current was measured using a Bell Sensor (type IF-5020P Series) measuring the current on the anode line.

E. Experimental Conditions

All measurements mentioned above were taken at three different mass flow rates: 5, 8, and 20 mg/s. For each of the three mass flow rates, measurements were taken for applied-magnetic-field values between 0 and 0.08 T, and total thruster current values between approximately 100 and 800 A and within the limits of the power supply. A total of 136 different cases with and without an applied magnetic field were studied. All magnetic field values were measured at the center of the solenoid.

III. Experimental Observations

Total power and thrust power are used to estimate thruster efficiency, as seen in the expression

$$\eta = \frac{P_{\text{acc}}}{P_{\text{tot}}} = \frac{\dot{m}u_e^2}{2P_{\text{tot}}} = \frac{T^2}{2J\dot{m}V_{\text{tot}}} \tag{1}$$

where V_{tot} is the total voltage, and $V_{\text{emf}} = T^2/(2J\dot{m})$ is the backelectromotive voltage. Therefore, aside from measuring the current, mass flow rate, and voltage, a knowledge of the scaling of thrust with the current is needed in order to calculate the sought η-J scaling.

For that, we employ a semiempirical thrust model derived and verified experimentally by Tikhonov et al. [2]. Tikhonov et al.'s thrust relation, shown next, was formulated based on an experimental study conducted on the same 30 kW LiLFA we used in our study as well as on higher power (greater than 100 kW) versions of this thruster [14–16]:

$$T(J) = K_{\text{self}}J^2 + K_H(2r_a)B_aJ + K_{\text{gd}}\dot{m}a_0 \tag{2}$$

Here, B_a is the applied magnetic field at the anode face ($B_a = B_c/2$ in the LiLFA) and a_0 is the sonic speed at the cathode exit. For the sonic speed, we take $a_0 = \sqrt{k(\gamma_e T_e + \gamma_i T_i)/m_i}$ with the electron, and ion temperatures equal 1.5 eV at the cathode exit, as was measured by Tikhonov et al. [2] using probes. We assume that $T_e = T_i$ based on the fact that, in AF-MPDTs, both temperatures were shown to be at the same order of magnitude [17]. We also assume that the specific heat ratio is taken to be that of a monatomic gas ($\gamma = 5/3$). The sonic speed is therefore $a_0 = 8.3 \times 10^3$ m/s. K_{self}, K_H, and K_{gd} are the self-field, Hall, and gas dynamic thrust coefficients and have the values

$$K_{\text{self}} = \left[\frac{3}{4} + \ln\left(\frac{r_a}{r_c}\right)\right] \times 10^{-7} = 1.76 \times 10^{-7}$$

$K_H = 0.1$, and $K_{\text{gd}} = 1.6$ given by Tikhonov et al. [2].

In Eq. (2), the first term represents the self-field component of thrust, the second term represents the applied-field component (which scales as the product JB_a), and the third term represents the gas dynamic contribution. We note that, since the sonic speed (a_0) is a function of temperature (T_e and T_i), it is also a function of current since an increase in current might lead to an increase in T_e. It was shown in previous studies on self-field [18] and AF-MPDTs [19] that the electron temperature has a weak dependence on current, and therefore so does the sonic speed, which is proportional to the square root of the electron temperature. We therefore assume for simplicity that the sonic speed is constant with the current.

We note that the AF-MPDT is designed to operate at current regimes in which the self-induced magnetic field generates thrust values that are negligible compared with the applied-field and gas dynamic thrust components. The mathematical dependence of thrust on current and applied magnetic field was formulated by using data from the 30, 150, and 200 kW lithium-fed AF-MPDTs [10,14,15,20,21] for a variety of current, applied-field, and mass-flow-rate values. The constants K_{self}, K_H, and K_{gd} in Eq. (2) were verified [10] by comparing Eq. (2) to experimental data taken at MAI on the 30 kW LiLFA, as shown in Fig. 3. It can be seen that, while a few of the experimental data points do not coincide very well with the model's curves, the thrust model does depict the trends correctly and can be used to estimate, to within 9%, the thrust generated by the 30 kW LiLFA at different operating conditions. It should also be noted that the experimental data are limited to current values higher than 400 A; therefore, any analysis conducted at lower current values using extrapolation from these data should be regarded with caution.

It is important to note that, even though the Tikhonov semiempirical thrust model [2,10] was derived for the lithium MPD thruster class built in MAI, it captures the same trends observed when operating other AF-MPDTs in other facilities at a variety of thruster power values, thruster geometries, and propellants [17,22–25]. These trends show a linear increase of thrust with an increase in the product JB. This repetitive trend for a vast number of different conditions implies a similar physical mechanism behind the thrust generation in AF-MPDTs. We can therefore assume that the effect that these linear trends in thrust have on trends in efficiency are similar in other types of thrusters operating in a variety of conditions. At the same time, we emphasize that the thrust scaling mechanism behind AF-MPDT is not yet understood for all current regimes, especially at low current values (where Mikellides and Turchi reported a $\sqrt{JB}$ scaling [11]), and so this empirical formulation should not be regarded as universal for all types of AF-MPDTs at all current regimes.

Given the lack of validation of the Tikhonov thrust model [10] at low currents, we checked the trends of efficiency at the low current regime while assuming the Mikellides thrust relation [11]. This examination produced the same trends as observed by using extrapolation to Tikhonov's thrust model.

To verify similar operating conditions in both the MAI and Princeton University facilities, we present in Table 1 a comparison between the voltage data obtained in both facilities at different current, applied-field, and mass-flow-rate cases. It can be seen from the table that MAI's voltage measurements are close to the expected range of the data obtained in this study, thus verifying operating

Table 1 Comparison between voltage measurements taken at MAI and Princeton University facilities

			Voltage, V		
$\dot{m}$, mg/s	B_c, T	J, A	MAI	Princeton	Difference, %
8	0.056	400	29.5	33 ± 2	11.9
8	0.056	500	33	34 ± 2	3
8	0.056	600	35	36 ± 2.5	2.9
8	0.056	700	39	39 ± 2.5	0
8	0.112	400	42	44 ± 3	4.8
8	0.112	500	46	47 ± 3	2.2
20	0.1	500	37.5	40 ± 2	6.7

repeatability between the two facilities. In addition, vacuum chamber ambient pressure was similar in both facilities and under 1 mT.

In Figs. 4–6, we present the voltage-current characteristics obtained for various applied-magnetic-field and mass-flow-rate values. In Figs. 7–9, we present the corresponding efficiencies calculated according to Eq. (1).

In Figs. 4–6, the sources of errors are due to small fluctuations in the measured voltage. Although the arc was stable during thruster operation, small fluctuations on the order of 1 V were observed in most cases. In addition, we observed that, for operation at higher current values, the range of voltage fluctuations was larger.

It can be observed from the figures that, for all cases presented, both the voltage and efficiency increase with increasing magnetic field. For the case of $\dot{m} = 5$ mg/s, the efficiency increases by as much as 150% from $\eta = 10\%$ to $\eta = 25\%$ at $J = 600$ A. This increase in efficiency is higher for low mass-flow-rate values; that is, the lower the mass flow rate, the greater the increase in efficiency with the applied field.

The mass flow rate also affects the slope of the voltage-current curves. The lower the mass flow rate, the greater the slope. The voltage-current curves at $\dot{m} = 20$ mg/s are flatter than at $\dot{m}=$ 5 mg/s. We can therefore conclude that the efficiency and total voltage are more sensitive to changes in current and applied magnetic field at low mass-flow-rate values.

It can also be observed that, for all cases presented, both the voltage and efficiency have decreasing–increasing trends with increasing current. Therefore, each curve has a minimum point. Moreover, the minimum point moves to lower current values with an increasing applied field while moving to higher current values with an increasing mass flow rate.

While the uncertainty at the low current regime cannot be accurately estimated, we checked on the trends in η-J data by using both the extrapolated Tikhonov thrust model [10], presented in Fig. 3, and the Mikellides thrust relation [11], which passes through the point $(0, T_0)$ in the T-J graph, where T_0 is the cold thrust. We observed the decreasing trends at low currents in both models. This

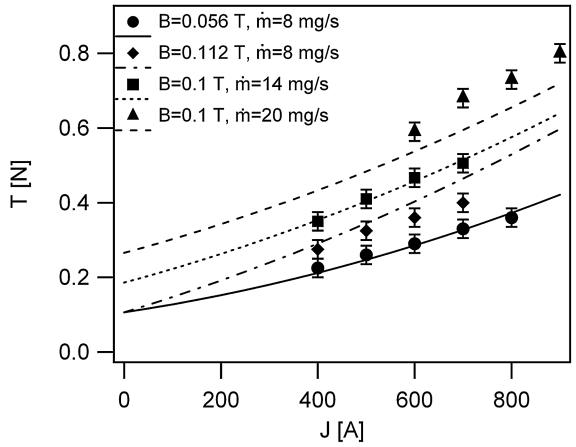

Fig. 3 Thrust measurements taken at MAI on the 30 kW LiLFA along with the Tikhonov semiempirical model [2,10].

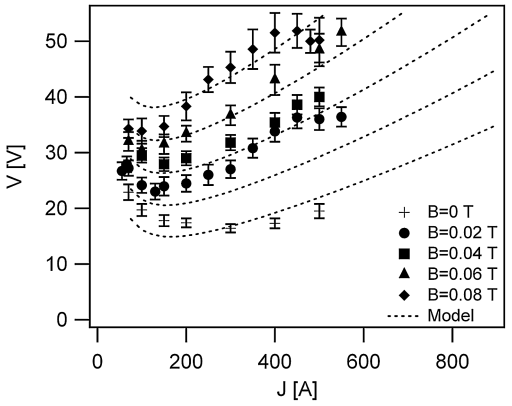

Fig. 4 Voltage-current characteristics for $\dot{m} = 5$ mg/s. Dashed lines represent the semiempirical voltage model represented by Eq. (4).

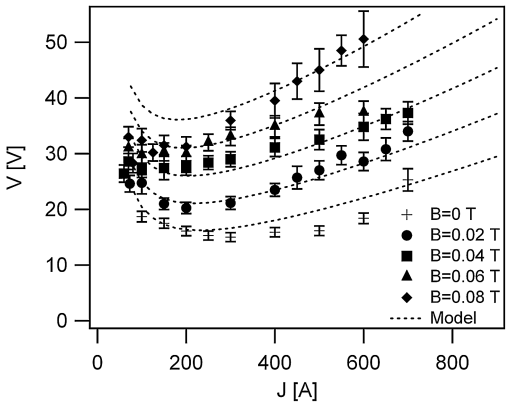

Fig. 5 Voltage-current characteristics for $\dot{m} = 8$ mg/s. Dashed lines represent the semiempirical voltage model represented by Eq. (4).

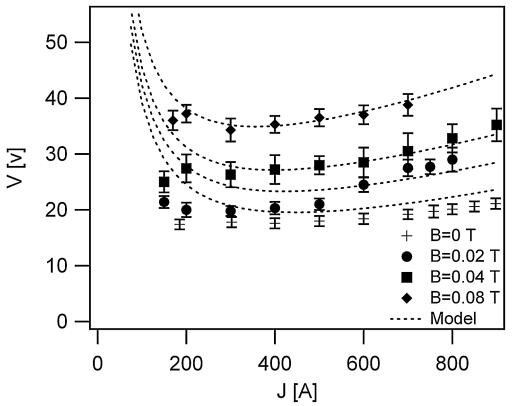

Fig. 6 Voltage-current characteristics for $\dot{m} = 20$ mg/s. Dashed lines represent the semiempirical voltage model represented by Eq. (4).

strengthens the assumption that, even though no thrust data exist for Tikhonov's model at low current, the thrust model still captures the qualitative trends in efficiency at the low current regime.

The observed trends are summarized in Table 2.

IV. Semiempirical Voltage Model

To analyze and understand the observed trends in voltage and efficiency, we develop a semiempirical voltage model.

The total voltage in MPDTs can be divided into three components as follows:

$$V_{\text{tot}} = V_{\text{res}} + V_{\text{emf}} + V_E \tag{3}$$

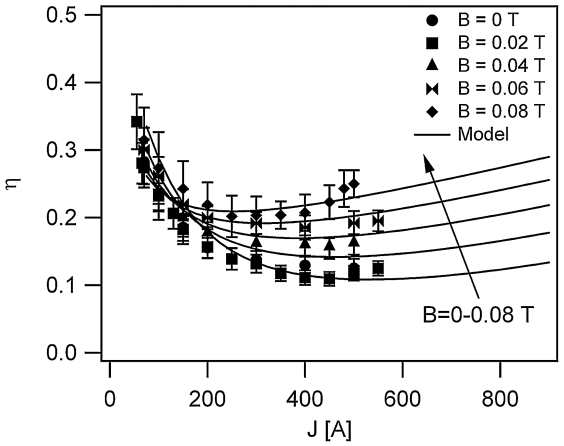

Fig. 7 Efficiency vs current for $\dot{m} = 5$ mg/s. Solid lines represent efficiency based on the semiempirical thrust and voltage models represented by Eqs. (2) and (4), respectively.

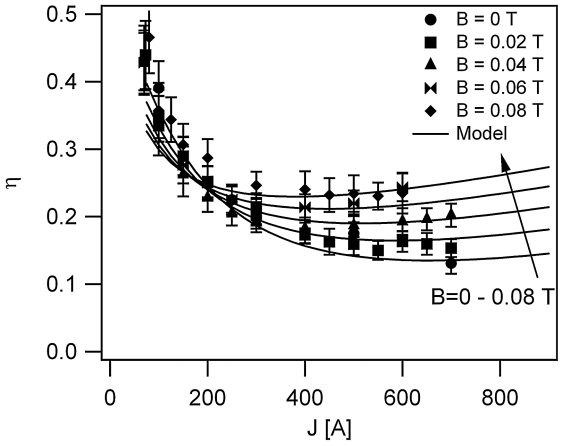

Fig. 8 Efficiency vs current for $\dot{m} = 8$ mg/s. Solid lines represent efficiency based on the semiempirical thrust and voltage models represented by Eqs. (2) and (4), respectively.

where V_{tot} is the total voltage between the anode and cathode. The first term on the right hand side V_{res} represents the resistive component of the voltage and is affected by the total current, the plasma density, and the plasma temperature. The second term V_{emf} represents the back electromotive voltage and originates from the motion of the plasma through regions of the finite magnetic field. The

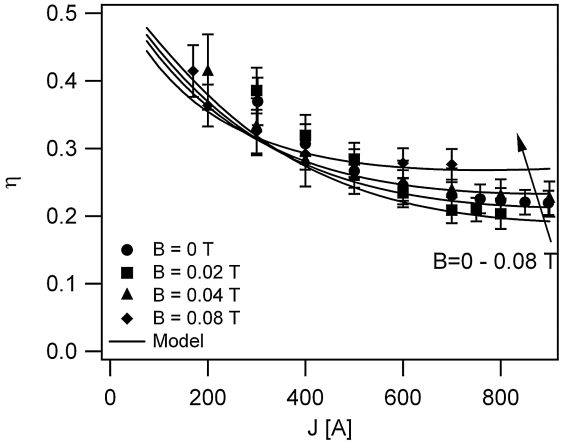

Fig. 9 Efficiency vs current for $\dot{m} = 20$ mg/s. Solid lines represent efficiency based on the semiempirical thrust and voltage models represented by Eqs. (2) and (4), respectively.

Table 2 Summary of observed trends in voltage-current and efficiency-current curves

	Observations
1	Both voltage (V) and efficiency (η) increase with applied magnetic field (B) for all values of current (J) and mass flow rate ($\dot{m}$).
2	Both voltage (V) and efficiency (η) are more sensitive to changes in current (J) and applied magnetic field (B) at low mass-flow-rate ($\dot{m}$) values.
3	Both voltage (V) and efficiency (η) exhibit a decreasing–increasing behavior with increasing current (J) for all applied-magnetic-field (B) and mass-flow-rate ($\dot{m}$) values. Each η-J curve has a minimum associated with it.
4	The minimum point moves to lower current (J) values with increasing applied field (B). The minimum point moves to higher current (J) values with decreasing mass flow rate ($\dot{m}$).

backelectromotive voltage drop is affected by the total current, plasma velocity, applied magnetic field, and mass flow rate. The third term V_E represents the voltage due to electrode losses in the anode and cathode sheaths. This mechanism was investigated in the past in self-field MPDTs [26] and AF-MPDTs [27,28]. In AF-MPDTs, it was shown [27] that the anode voltage drop scales linearly with the applied magnetic field B and the applied current J and has a weak inverse dependence on the mass flow rate.

Based on previous studies and our present investigation, we constructed the following model for the total voltage:

$$V_{\text{tot}} = \frac{1}{J}\frac{\dot{m}\epsilon_i}{m_i} + \frac{1}{J}\frac{T^2}{2\dot{m}} + \phi_W + \frac{(C_1 J(C_2 + B_a) + C_3 B_a)}{\dot{m}^n} \quad (4)$$

The first term represents the ionization voltage, which scales inversely with current. Since, energetically speaking, the ionization process in MPDTs is maintained via resistive heating, this term is part of the resistive heating voltage component. The plasma is assumed to be fully singly ionized with an ionization potential of $\epsilon_i = 5.391$ eV. This assumption is based on past research conducted in self-field MPDTs [29–31]. The second term represents the backelectromotive voltage component and is discussed next. The third term represents the electrodes' work function. Lithium-coated tungsten has a work function of approximately 2.5 eV [8]; thus, $\phi_W \simeq 5$ eV for the anode and cathode combined. The last term represents the electrodes' voltage fall and resistive heating (not including ionization). The mathematical form of the last term and the four constants (C_1, C_2, C_3, and n) were found by obtaining the best fit of the above expression to the measured voltage-current characteristics. This yielded the following values: $C_1 = 6.18 \times 10^{-4}$, $C_2 = 0.1$, $C_3 = 0.9272$, and $n = 0.5$. The applied field in this expression is measured at the anode face due to the significance that the anode voltage fall has on this term in MPDTs [27]. For simplicity, we refer to the sum of all voltage components, not including the backelectromotive component as the nonuseful voltage, since it represents the sum of the voltages associated with all power losses in thruster operation.

We employ the Tikhonov thrust expression [Eq. (2)] in order to obtain a mathematical expression for the backelectromotive voltage component (V_{emf}) [2]. All three thrust components will therefore have an effect on the backelectromotive voltage, as can be seen in the following expression [Eq. (5)]:

$$V_{\text{emf}} = \frac{K_{\text{gd}}^2}{2} a_0^2 \frac{\dot{m}}{J} + K_{\text{gd}} K_H a_0 (2r_a) B_a + \frac{K_H^2 (2r_a)^2}{2} \frac{B_a^2 J}{\dot{m}} + K_{\text{gd}} K_{\text{self}} a_0 J + K_H K_{\text{self}} (2r_a) \frac{B_a J^2}{\dot{m}} + \frac{K_{\text{self}}^2}{2} \frac{J^3}{\dot{m}} \quad (5)$$

The first three terms represent the contribution of the gas dynamic and applied-field component to thrust. The last three components represent the contribution of the self-field component of thrust and are negligible at current values less than about 800 A.

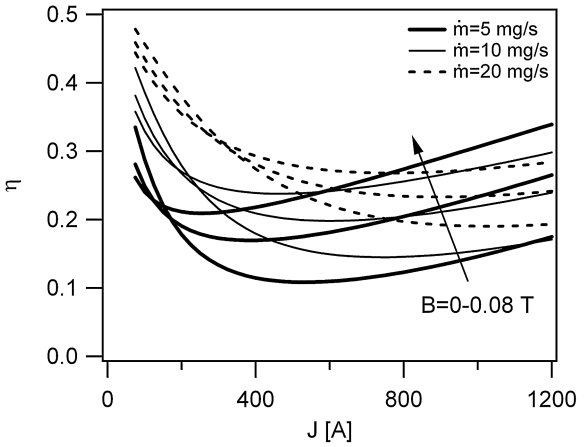

Fig. 10 Efficiency vs current for various applied-field and mass-flow-rate values based on the semiempirical thrust and voltage models represented by Eqs. (2) and (4), respectively.

Using Eqs. (4) and (5), we plot in Fig. 10 the efficiency-current curves for different applied-magnetic-field and mass-flow-rate values.

Armed with the preceding mathematical expressions, we can now analyze the observed trends in voltage and efficiency.

V. Physical Interpretation

The first, and probably most important, observation made is the fact that, except for at a low current operating regime, the efficiency increases with increasing applied magnetic field. The reason for this behavior is found from Eqs. (4) and (5), where the efficiency is seen to be greater when the useful voltage component (V_{emf}) increases faster than the nonuseful voltage ($V_{\text{tot}} - V_{\text{emf}}$) with the applied magnetic field. Since V_{emf} scales with B^2 while the nonuseful voltage scales with B, there is a general increase of the efficiency with B. From the mathematical form of the last term in Eq. (4), we can conclude that the heating and electrode sheath power loses scale linearly with the applied field; therefore, the useful power increases faster than the nonuseful power with the increasing applied field.

From the semiempirical model, we conclude that the nonuseful voltage component scales linearly with the current (J) and applied magnetic field (B) and inversely with the square root of the mass flow rate ($\dot{m}$), as seen in Eq. (4). This result is important since it implies the following:

1)_The nonuseful voltage increases linearly with increasing current, much like in self-field MPDTs [26]. This phenomenon is attributed to electrode sheath losses and is still not fully understood. In addition, the anode voltage drop was measured by Myers and Soulas [27] and Meyers et al. [28] in AF-MPDTs and found to scale linearly with the current. This fact strengthens the inference that the observed trend is due to electrode sheath power loss.

2) The nonuseful voltage increases linearly with the increasing applied magnetic field. Although Myers and Soulas [27] found the anode loss to scale with the applied field, this phenomenon cannot be attributed to electrode sheath effects since the sheath length is of the order of the Debye length, which in MPDTs is on the order of 10^{-6} m, while the electron gyroradius is on the order of 10^{-4} m. Therefore, it is more likely that the voltage drop discussed is resistive and is due to a decreasing conductivity with an increasing applied magnetic field. With a decreasing conductivity, the thruster will require operation with higher voltage fall in order to achieve the desired current. To verify this assumption, one needs to estimate the conductivity using the generalized Ohm's law and measurements of the electric field and current density distributions: an elaborate and difficult process.

3) The conductivity change argument stated above might also explain the inverse dependence on the mass flow rate. An increase in mass flow rate will increase the electron number density (at a given input power density), thus increasing the conductivity and reducing the voltage required to sustain the desired current.

We also observed that the increase in efficiency with increasing current and applied field is more sensitive when the mass flow rate is lower. This can be corroborated with the fact that the backelectromotive voltage scales with $(JB^2)/\dot{m}$, as seen in the third term in Eq. (5). Any changes in current or applied field will be greater for lower values of mass flow rate. This means that the enhancement of the efficiency by the applied magnetic field is greater when the mass flow rate is reduced. Physically speaking, this can be explained as follows. As the current increases, so does the thrust, the exhaust velocity, and backelectromotive voltage. At a lower mass flow rate, any increase in current, and therefore thrust, leads to a greater increase in exhaust velocity, and thus to a higher back electromotive voltage.

The decreasing–increasing behavior of efficiency with increasing current can be explained by considering the contribution of each thrust component to the backelectromotive voltage. Each one of the three thrust components dominates thrust production in different current regimes. The thrust regime characterized by the lowest current values is the gas dynamic regime. This can be seen from Eq. (2) and Fig. 3, where it can be verified that, at low current values, the thrust consists mostly of the value of the current-independent constant $K_{\text{gd}}a_0\dot{m}$. The gas dynamic thrust component contributes the quantity $K_{\text{gd}}^2 a_0^2 \dot{m}/2J$ to the backelectromotive voltage, and therefore will decrease with increasing current. The reduction in this voltage component will contribute to the reduction in efficiency. When increasing the current even further, the applied-field component of thrust dominates the scaling of thrust. This can be seen in Fig. 3, where at intermediate current values, the thrust consists mostly of the value of the applied-field component $K_H(2r_a)B_aJ$. The applied-field thrust component contributes the quantity $K_H^2(2r_a)^2B_a^2J/2\dot{m}$ to the backelectromotive voltage, thus scaling linearly with the current, much like the nonuseful voltage. For this reason, the efficiency curve flattens out and rises when the self-field component of thrust becomes larger. The following asymptotic efficiency value can be calculated by taking the expression for efficiency at $J \to \infty$ and neglecting the self-field component of thrust:

$$\eta_{\text{asymptotic}} = \left[1 + \frac{C_1(B_a + C_2)\sqrt{\dot{m}}}{0.5(K_H(2r_a)B_a)^2}\right]^{-1} \tag{6}$$

We see that the asymptotic efficiency increases with increasing applied magnetic field and decreases with the mass flow rate. As mentioned above, further increases of the efficiency with the current are due to the effect of the self-field thrust component on the backelectromotive voltage. Since the latter scales with J^3 (which implies a vigorous increase with the total current) while the nonuseful voltage scales with J, the efficiency will rise with the current.

The current value at which the efficiency reaches its minimum value can be found by solving the equation $\partial\eta(J)/\partial J = 0$ for J. Since the mathematical expression for the solution for J_{min} is too large, it will not be quoted here, but we explain the physical mechanisms controlling the value of J_{min}. As explained above, the decreasing–increasing efficiency behavior is a result of the interplay between the magnitudes of the different thrust components at different current regimes. As seen in Eq. (5), high $\dot{m}$ will increase the first term ($\propto \dot{m}/J$) on the left-hand side, which corresponds to the gas dynamic thrust component, while decreasing the third term ($\propto J/\dot{m}$), which corresponds to the applied-field thrust component. Therefore, the recovery of the efficiency with the current will be pushed to higher current values. On the other hand, raising the applied magnetic field will not change the magnitude of the first term in Eq. (5), yet it will increase the second ($\propto B_a$) and third ($\propto B_a^2$) terms, thus pushing the minimum point to lower current values.

The above analysis and the efficiency curves presented in Fig. 10 imply that the optimal operational regime of the LiLFA is at the low current regime due to the high efficiencies associated with this regime. However, one must remember that the Tikhonov thrust model [2] used to derive the expression for efficiency is based on

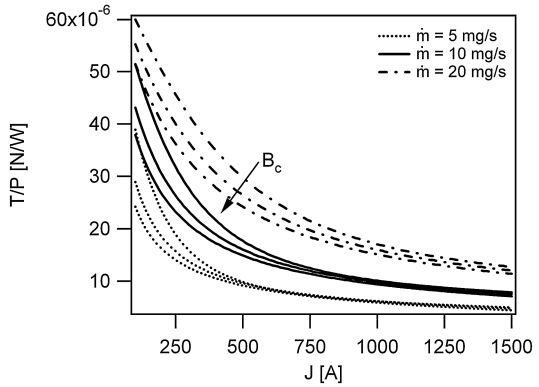

Fig. 11 Thrust-to-power ratio vs current for various applied-field and mass-flow-rate values.

experimental results at current values higher than 400 A. For this reason, any extrapolation of the model to a low current regime should be regarded with caution. In addition, at low current regime thrust, which increases monotonically with current, is lowest, thus the specific impulse is lowest since $I_{sp} = T/\dot{m}g_0$. For this reason, the low current regime is of low interest.

On the other hand, the high current regime is of great interest due to the high efficiencies and specific impulse associated with it. To illustrate the benefit of operating at a high current regime, it is useful to plot the thrust-to-power ratio, which equals

$$\frac{T}{P} = \frac{2\eta}{I_{sp}g_0} \tag{7}$$

against the current. T/P-J curves are plotted in Fig. 11. It can be seen from the figure that, as J is raised, T/P reaches an asymptotic value for each mass-flow-rate value. This gives a sense of the relative scaling of efficiency and specific impulse with the thruster's operational parameters.

VI. Conclusions

To shed light on the nature of the scaling of AF-MPDT performance with applied magnetic field, the voltage-current characteristics of a lithium-fed AF-MPDT were measured at various applied-magnetic-field and mass-flow-rate values, and a semiempirical thrust model was employed to obtain a mathematical expression for the thrust. Using the voltage data and the semiempirical thrust formula, the thruster's efficiency and its dependences on current, applied magnetic field, and mass flow rate were calculated. In addition, a semiempirical expression for the voltage was derived in order to characterize the nonuseful voltage.

It was found that the efficiency increases with increasing applied magnetic field. This increase was attributed to the scaling of thrust and the backelectromotive voltage with the applied magnetic field. This increase was found to be greater than the increase of the nonuseful voltage with the applied field.

The nonuseful voltage was found to scale linearly with the current and applied magnetic field, and inversely with the mass flow rate. It was suggested that the scaling with the current was due to sheath effects, as in self-field MPDTs, and the scaling with the magnetic field was due to a decrease in conductivity with an increasing applied magnetic field.

It was also found that the efficiency-current curve has a decreasing–increasing behavior, with a minimum point that is affected by both the applied magnetic field and the mass flow rate. It has been shown that the value of the current at this minimum point is higher when the mass flow rate increases and lower with an increase in the applied magnetic field. An expression for the asymptotic value of efficiency was derived, and it was shown that the minimum possible efficiency is larger for larger values of the applied magnetic field.

These findings can be used to derive guidelines for AF-MPDT design, performance scaling, and optimization in lithium-fed AF-MPDTs at power levels under 30 kW.

Acknowledgments

We acknowledge the support of the Plasma Science and Technology Program from the Princeton Plasma Physics Laboratory and the technical help of Robert Sorenson.

References

[1] Kodys, A. D., and Choueiri, E. Y., "A Critical Review of the State-of-the-Art in the Performance of Applied-Field Magnetoplasmadynamic Thrusters," 41st Joint Propulsion Conference, Tucson, AZ, AIAA Paper 2005-4247, 2005.

[2] Tikhonov, V. B., Semenikhin, S. A., Brophy, J. R., and Polk, J. E., "Performance of 130 kw MPD Thruster with an External Magnetic Field and Li as a Propellant," 25th International Electric Propulsion Conference, Cleveland, OH, IEPC Paper 97-117, 1997.

[3] LaPointe, M. R., Strzempkowski, E., and Pencil, E., "High Power MPD Thruster Performance Measurements," 40th Joint Propulsion Conference, Fort Lauderdale, FL, AIAA Paper 2004-3467, 2004.

[4] Maecker, H., "Plasma Jets in Arcs in a Process of Self-Induced Magnetic Compression," *Zeitschrift für Physik*, Vol. 141, 1955, pp. 198–216. doi:10.1007/BF01327300

[5] Jahn, R. G., *Physics of Electric Propulsion*, McGraw–Hill, New York, 1968, pp. 235–254.

[6] Choueiri, E. Y., "The Scaling of Thrust in Self-Field Magnetoplasmadynamic Thrusters," *Journal of Propulsion and Power*, Vol. 14, No. 5, 1998, pp. 744–753. doi:10.2514/2.5337

[7] Zuin, M., Cavazzana, R., Martines, E., Serianni, G., Antoni, V., Bagatin, M., Andrenucci, M., Paganucci, F., and Rossetti, P., "Critical Regimes and Magnetohydrodynamic Instabilities in a Magneto-Plasma-Dynamic Thruster," *Physics of Plasmas*, Vol. 11, No. 10, 2004, pp. 4761–4770. doi:10.1063/1.1786593

[8] Polk, J. E., and Pivirotto, T. J., "Alkali Metal Propellants for MPD Thrusters," AIAA/NASA/OAI Conference on Advanced SEI Technologies, Cleveland, OH, AIAA Paper 1991-3572, 1991.

[9] Ageyev, V. P., and Ostrovsky, V. G., "High Current Stationary Plasma Accelerator of High Power," 23th International Electric Propulsion Conference, Seattle, WA, IEPC Paper 93-117, 1993.

[10] Popov, G., Kim, V., Tikhonov, V. B., and Semenikhin, S., "The Second Quarterly Report on the Stage No. 3 c, d of the Contract on the Research Studies No. NASW-4851 Between RIAME MAI and NASA," Moscow Aviation Inst. TR, Moscow, April 1997.

[11] Mikellides, P. G., and Turchi, P. J., "A Theoretical Model for the Thrust and Voltage of Applied-Field MPD Thrusters," 34th Joint Propulsion Conference, Cleveland, OH, AIAA Paper 1994-3474, 1998.

[12] Kodys, A. D., Emsellem, G., Cassady, L. D., Polk, J. E., and Choueiri, E. Y., "Lithium Mass Flow Control for High Power Lorentz Force Accelerators," 2001 Space Technology and Applications International Forum, Albuquerque, STAIF Paper E08-195, 2001.

[13] Cassady, L. D., "Lithium-Fed Arc Multichannel and Single-Channel Hollow Cathode: Experiment and Theory," Ph.D. Thesis, Princeton Univ., Princeton, NJ, 2006.

[14] Popov, G., Kim, V., Tikhonov, V. B., and Semenikhin, S., "The Second Quarterly Report on the Stage No. 3 b of the Contract on the Research Studies No. NASW-4851 Between RIAME MAI and NASA," Moscow Aviation Inst. TR, Moscow, Dec. 1996.

[15] Popov, G., Kim, V., Tikhonov, V. B., and Semenikhin, S., "The First Quarterly Report on the Stage No 3 a of the Contract on the Research Studies No. Nasw-4851 between RIAME MAI and NASA," Moscow Aviation Inst. TR, Moscow, April 1996.

[16] Popov, G. A., Kim, V., Tikhonov, V. B., Semenikhin, S. A., and Tibrina, M. K., "The Third Quarterly Report on the Milestones (a)(4) and (a)(5) (d) of Sow of Contract No. 960938 Between RIAME MAI and JPL," Moscow Aviation Inst. TR, Moscow, Dec. 1998.

[17] Fradkin, D. B., "Analysis of Acceleration Mechanisms and Performance of an Applied Field MPD Arcjet," Ph.D. Thesis, Princeton Univ., Princeton, NJ, 1973.

[18] Tahara, H., Kagaya, Y., and Yoshikawa, T., "Exhaust Plume Characteristics of Quasi-Steady MPD Thrusters," 27th International Electric Propulsion Conference, Pasadena, CA, AIAA Paper 2001-133, 2001.

[19] Myers, R. M., "Plume Characteristics of MPD Thrusters: A Preliminary Examination," 25th Joint Propulsion Conference, Monterey, CA, AIAA Paper 1989-2832, 1989.
[20] Popov, G., Kim, V., Tikhonov, V. B., and Semenikhin, S., "The Second Quarterly Report on the Stage No. 2 a of the Contract on the Research Studies No. NASW-4851 Between RIAME MAI and NASA," Moscow Aviation Inst. TR, Moscow, July 1996.
[21] Popov, G. A., Kim, V., Tikhonov, V. B., Semenikhin, S. A., and Tibrina, M. K., "The Third Quarterly Report on the Milestones (a)(3) and (a)(5) (c) of Sow of Contract No. 960938 Between RIAME MAI and JPL," Moscow Aviation Inst. TR, Moscow, June 1998.
[22] Mantenieks. M. A., Sovey, J. S., Myers, R. M., Haag, T. W., Raitano, P., and Parkes, J. E., "Performance of a 100 kw Class Applied Field MPD Thruster," 25th Joint Propulsion Conference, Monterey, CA, AIAA Paper 1989-2710, 1989.
[23] Myers, R. M., Mantenieks, M., and Sovey, J., "Geometric Effects in Applied-Field MPD thrusters," 21st International Electric Propulsion Conference, Orlando, FL, AIAA Paper 1990-2669, 1990.
[24] Fradkin, D. B., and Roehling, D. J., "Thrust Stand Performance of a Lithium Fueled Applied Field MPD Arcjet," *13th Symposium on the Engineering Aspects of Magnetohydrodynamics*, Stanford Univ., No. VI.11., Stanford, CA, 1973, pp. 1–5.
[25] Tahara, H., Takiguchi, F., Kagaya, Y., and Yoshikawa, T., "Performance Characteristics and Discharge Features of a Quasi-Steady Applied-Field MPD Arcjet," 21st International Electric Propulsion Conference, Orlando, FL, IEPC Paper 1991-0073, 1991.
[26] Diamant, K. D., Choueiri, E. Y., and Jahn, R. G., "Spot Mode Transition and the Anode Fall of Pulsed MPD Thrusters," *Journal of Propulsion and Power*, Vol. 14, No. 6, 1998, pp. 1036–1042. doi:10.2514/2.5371
[27] Myers, R. M., and Soulas, G. C., "Anode Power Deposition in Applied-Field MPD Thrusters," 28th Joint Propulsion Conference, Nashville, TN, AIAA Paper 1992-3463, 1992.
[28] Myers, R. M., Gallimore, A. D., and Jahn, R. G., "Anode Power Deposition in an Applied-Field Segmented Anode MPD Thruster," *Journal of Propulsion and Power*, Vol. 10, No. 2, 1994, pp. 262–268. doi:10.2514/3.23738
[29] Randolph, T. M., Von Jaskowsky, W. F., Kelly, A. J., and Jahn, R. G., "Ionization Processes in the Interelectrode Region of an MPD Thruster," 22nd International Electric Propulsion Conference, Viareggio, Italy, AIAA Paper 1991-0052, 1991.
[30] Choueiri, E. Y., and Randolph, T. M., "Ionization Front in a High-Current Gas Discharge," *Physics of Plasmas*, Vol. 14, No. 3, 2007, Paper 033502. doi:10.1063/1.2646365
[31] Sankaran, K., "Simulation of Plasma Flows in Self-Field Lorentz Force Accelerators," Ph.D. Thesis, Princeton Univ., Princeton, NJ, 2005.

L. King
Associate Editor